Article

Experimental and Theoretical Analysis of Flexural Properties of Mortar Beam Reinforced with Coated Carbon-Fiber Textile

Geuntae Hong [1], Jangsoon Park [2], Seong-Cheol Lee [1], Soo Won Cha [3], Jaewoo Ryu [4] and Seongcheol Choi [4,*]

1 Department of Civil Engineering, Kyungpook National University, 80 Daehak-ro, Buk-gu, Daegu 41566, Republic of Korea; gthong@knu.ac.kr (G.H.); seonglee@knu.ac.kr (S.-C.L.)
2 Songsan Green City Project Office, Korea Water Resources Corporation, 6-50 Dongi-Gil, Hwaseong-si 18245, Gyeonggi-do, Republic of Korea; jsoon@kwater.or.kr
3 Department of Civil and Environmental Engineering, University of Ulsan, 93 Daehak-ro, Nam-gu, Ulsan 44610, Republic of Korea; chasw@ulsan.ac.kr
4 Department of Civil and Environmental Engineering, Chung-Ang University, 84 Heukseok-ro, Dongjak-gu, Seoul 06974, Republic of Korea; yjw1648@naver.com
* Correspondence: schoi@cau.ac.kr; Tel.: +82-2-820-5303

Abstract: The flexural behavior of mortar beams reinforced with coated carbon-fiber textile was experimentally analyzed in this study. Accordingly, pull-out and bending tests were performed on textile-reinforced mortar (TRM) beam specimens. The experimental results demonstrated the superior bond performance of the coated carbon-fiber textile. The TRM beam exhibited sufficient ductility even after the occurrence of flexural cracks. In addition, a theoretical analysis method for predicting the flexural behavior of a TRM beam was established based on the experimentally determined bond behaviors of the textile reinforcement in cementitious materials. The analysis demonstrated that the bending behavior of the TRM beam was reasonably predicted. The results of this study can serve as basic data for the structural application of textile-reinforced cementitious composites.

Keywords: carbon-fiber textile; flexural behavior; pull-out; reinforcement; textile-reinforced mortar (TRM)

1. Introduction

Reinforcing bars are used in concrete to remediate the weak tensile strength of the latter. Reinforcing bar corrosion is the most dominant factor in reducing the long-term structural performance and durability of reinforced concrete (RC) structures. To prevent it, existing design standards stipulate a minimum cover thickness for the reinforcing bar according to the type of structure and exposure environment [1,2]. However, despite exceeding the minimum cover thickness, corrosion in the reinforcing bar is accelerated when the concrete cracks due to exposure to the external environment [3–5]. In addition, even though the concrete cover occupies a part of the structure cross-section, the design can be inefficient because its contribution to the load-bearing capacity of the structure is limited by cracking [6,7].

Over the past few decades, researchers have proposed concrete reinforced with discontinuous short fibers [8,9] or continuous fiber textile [10,11] as a substitute or strengthening materials to overcome the crack vulnerability and the resulting decrease in the durability of existing plain concrete and RC structures. Fiber-reinforced composite (FRC) is a composite material comprising discontinuous short fibers with random orientations in the cement matrix. FRC allows for the facile inclusion of fibers in the mixture, effectively improves crack propagation resistance of the cement matrix, effectively strengthens the toughness by fiber bridging, and is cost effective [12–16]. On the other hand, because the FRC performance may depend on the dispersion of fibers, various methods for improving this aspect have been studied [9]. Textile-reinforced mortar (TRM) is a composite material comprising a noncorrosive textile mesh in the cement matrix. Weight reduction is achieved by reducing

the cover thickness because the textile is corrosion resistant. In addition, it is suitable for structures subjected to tensile or bending loads because it has excellent corrosion resistance even when the concrete is cracked and exposed to corrosive environments [17,18]. In particular, because the continuous fiber textiles are embedded in a fixed position, the fiber efficiency under tension after cracking is maximized. Therefore, TRM can solve the problems inherent in existing fiber-reinforced cementitious composites [10,11], which have variability in tensile behavior after cracking due to differences in the direction, length, and distribution of fibers exposed to cracks [19,20].

Currently, the main textile yarns used in TRM are carbon, alkali-resistant glass, and basalt, which have high strength, stiffness, and corrosion resistance [10,11,18,21]. In particular, carbon fiber is more costly than other fibers but has superior mechanical properties, such as elastic modulus and tensile strength. Accordingly, numerous studies are underway to verify the feasibility of using carbon fiber as a strengthening material for plain concrete and RC structures [9,22]. However, the flexural behavior of carbon-textile-reinforced concrete has not been adequately evaluated. Most studies have focused on the use of fiber textiles as a structural reinforcement to improve the performance of concrete [11]. These studies have evaluated improvements in the mechanical behavior (flexural bonding behavior, etc.) of TRM through experimental analysis. However, only a few studies have analyzed the bonding behavior of coated carbon textile in concrete and the flexural behavior of coated carbon-textile-reinforced cementitious materials [23,24]. In addition, although the research results [11] have suggested that TRM can improve performance under serviceability loads by increasing the flexural and shear capacity compared to existing RC members, the field application of TRM as a structural member necessitates a concise and reliable analysis model to predict the structural behavior of TRM. Recently, in studies by [25–27], the bonding behavior (bond–slip relationship) of carbon textile reinforcement in concrete was calibrated and evaluated through numerical analysis using DIANA, a finite element analysis software. Afterward, a four-point bending test of the carbon-textile-reinforced concrete slab was simulated to evaluate the flexural behavior, and the simulated results were compared with the experimental results. Nevertheless, research on a theoretical analysis model that can predict the flexural behavior of coated carbon-textile-reinforced concrete is lacking [28,29], and the actual bonding behavior of textiles in a cement matrix was not directly considered for flexural analysis. To fill this gap, the bond behavior is directly considered in the flexural analysis in this study.

Accordingly, this study aims to experimentally and analytically investigate the structural behavior of a coated carbon-fiber textile in cementitious materials, along with its viability for tensile reinforcement. In the experiment, a carbon-fiber textile coated with low-viscosity epoxy resin was used. To analyze the bond–slip relationship of the coated carbon-fiber textile in cementitious materials, a mortar specimen embedded with one layer of coated textile mesh was fabricated, and a direct pull-out test for textile roving was performed. In addition, a mortar beam reinforced with coated carbon-fiber textile in the tensile zone was fabricated, and the deflection due to the added load before and after cracking was measured through a four-point bending test to analyze the flexural behavior. Furthermore, a theoretical analysis method for predicting the flexural behavior before and after cracking was proposed by idealizing the failure mode of the mortar beam reinforced with coated carbon-fiber textile based on the bonding behavior of the coated carbon textile, which was experimentally measured. Subsequently, the predicted flexural behavior of the mortar beam reinforced with coated carbon-fiber textile from the analysis was compared with the experimental results.

2. Experiment

2.1. Materials

Table 1 lists the properties of the cementitious mixture used in the mortar beam specimens with a coated carbon-fiber textile for analyzing its bond behavior and flexural strengthening effect. Type-I ordinary Portland cement (OPC; CEM I, Sungshin Cement,

Seoul, Republic of Korea) with a Blaine fineness of 3300 cm^2/g was mixed with standard sand and water in compliance with ISO 679 [30]; polycarboxylate superplasticizer (SP8HU, BASF, Ludwigshafen, Germany) was also added to the mortar mixture. The mixing procedure adhered to ISO 679 [30]. The mortar compressive strength after 28 days was measured in accordance with ASTM C873/C873M [31] to be 42.0 ± 1.2 MPa, and the elastic modulus was measured in compliance with ASTM C469/C469M to be 26.2 ± 0.1 GPa [32].

Table 1. Composition of the cementitious mortar mixtures used in the test.

W/C [%]	Cement [kg/m^3]	Water [kg/m^3]	Sand [kg/m^3]	SP [1] [kg/m^3]
47	480	226	1625	1

[1] Superplasticizer.

Various mixture compositions for the TRC have been developed according to the required workability and bonding behavior of the textile reinforcement, among others. Accordingly, a water/cement (w/c) ratio of approximately 0.4 is generally utilized [33]. In addition, previous studies have reported that the fiber–matrix bond may decrease with increasing w/c [34,35]. Therefore, in this study, a relatively high w/c was used for the TRM to conservatively evaluate the bond performance of the coated carbon-fiber textile. The textile used may exhibit better bond performance at low w/c, but further study is needed in this area.

Figure 1 shows the carbon-fiber textile used in this study, which was manufactured by Shanghai Lishuo Composite Material Technology Co., Ltd. (Shanghai, China). The average mesh size and clear spacing between the rovings of the carbon-fiber textile used in this study were approximately 14 mm and 12 mm, respectively. Because the outer surface of the carbon-fiber textile supplied by the manufacturer had no separate coating, the textile was additionally coated with a low-viscosity epoxy resin to improve bonding to the cement matrix. In addition, the carbon-fiber textile could easily be fixed inside the specimen because the coating increased the rigidity. Table 2 lists the material properties of the carbon-fiber roving used in textiles provided by the manufacturer. However, the geometry of each roving of the textile used in the test differs slightly, as shown in Figure 1. Accordingly, there may be uncertainty about the properties of Table 2.
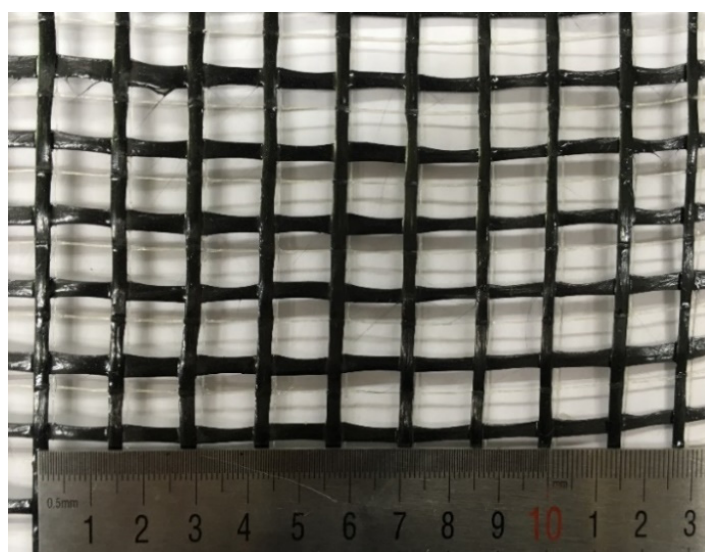

Figure 1. Coated carbon-fiber textile.

Table 2. Properties of the carbon-fiber roving used in the textile.

Cross-Sectional Area [mm^2]	Perimeter [mm]	Tensile Strength [MPa]	Young's Modulus [GPa]	Density [g/cm^3]
0.85	3.88	4300	240	1.7

2.2. Direct Pull-Out Test

The TRM fabricated in this study is a composite of carbon-fiber textile and cement mortar, and the bond behavior between the cement matrix and the textile mesh has a very important influence on the structural behavior of TRM [36]. Previous studies [24–26] have adopted a single- or double-sided test to investigate the bond stress–slip relationship of TRM. The single-sided test was performed by embedding both ends of a single yarn in an epoxy resin and cement matrix [37]. However, this type of test is not reflective of the behaviors of a textile mesh because it utilizes a single yarn. The double-sided test is advantageous because an asymmetric embedded length can be applied. Moreover, because the test is conducted by directly embedding the textile mesh, the effect of the mesh shape can also be considered [38].

Therefore, a double-sided unsymmetrical pull-out test was performed in this study to investigate the bond stress–slip relationship in TRM. Figure 2 shows the geometry and preparation of the pull-out test specimen based on the test set-up designed by Krüger [39]. The specimen dimensions were 300 × 100 × 20 mm^3, and a layer of textile mesh was embedded in the middle of the mortar specimen. The reinforcement embedment length was asymmetrically set to 25 mm and 50 mm through saw cutting. Double-sided saw cutting ensured the upper anchoring area was constrained by a specific positioning of a predetermined breaking point. Additionally, a chosen anchoring length of 225 mm in the lower part of the specimen is generally sufficient for secure anchoring [39]. To ensure a consistent embedded height of the mesh in the specimen, the edge of the textile mesh was fixed to the mold before casting. In general, the peak load of the prestressed TRM increases as the slip decreases, resulting in brittle behavior [38]. Therefore, embedding at the correct position was carefully ensured to prevent generating pretensile force and to prevent bending while installing the textile mesh in the specimen, thus minimizing the prestress that may occur in the textile mesh. The specimen was demolded 24 h after casting, followed by curing in water for 28 days at 20 ± 0.5 °C.
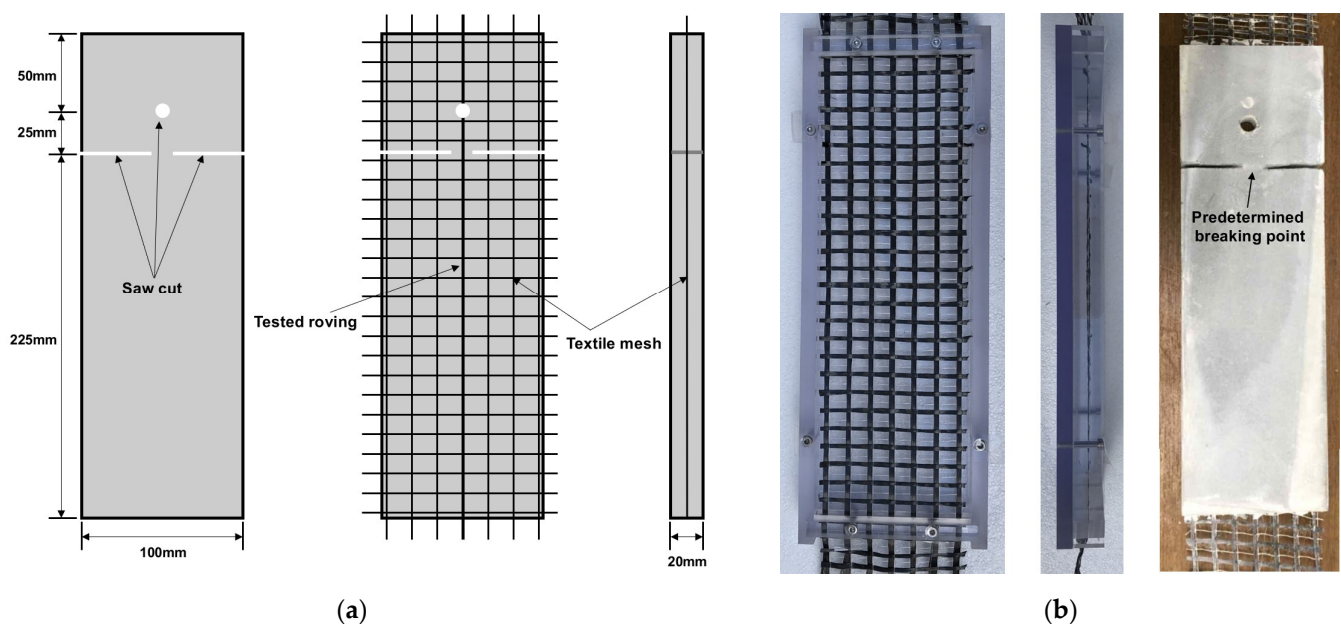

(**a**)   (**b**)

Figure 2. (**a**) Geometry and (**b**) preparation of the pull-out test specimen.

Figure 3 shows the pull-out test setup. Tensile stress was applied to the specimen through iron clamps fixed at both ends of the specimen. The inner surface of the clamp was roughened to prevent slip between the specimen and the clamp. Linear variable displacement transformers (LVDTs) were installed on both sides of the center of the specimen to measure the opening displacement between the upper and lower parts of the specimen under the tensile load, which is representative of the pull-out displacement of the coated carbon-fiber textile reinforcement. The pull-out test was conducted under displacement control at a speed of 1 mm/min, and the applied load and LVDT displacement were measured and recorded every second.
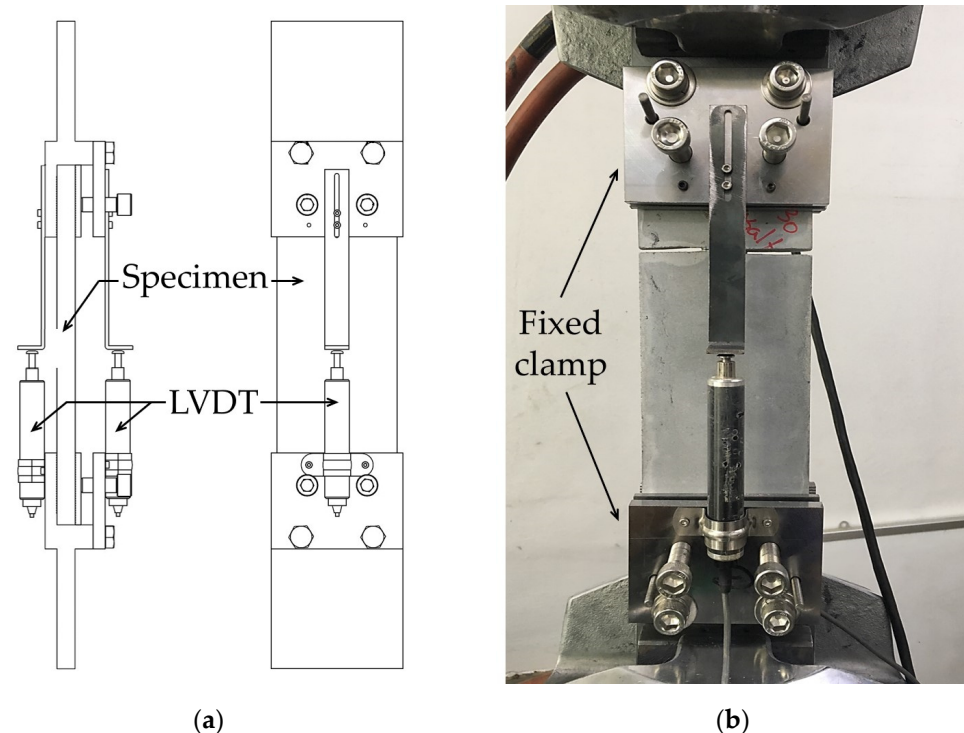

(**a**)   (**b**)

Figure 3. Experimental setup for the pull-out test. (**a**) Schematics and (**b**) pull-out test specimen mounted on a universal testing machine.

2.3. Four-Point Bending Test

To analyze the reinforcement effect of the coated carbon-fiber textile on the structural behavior of the TRM beam, a four-point bending test was performed in accordance with ASTM C1609/C1609M [40] to measure the load–deflection behavior. Accordingly, $100 \times 100 \times 400$ mm^3 specimens were prepared for the test. The layer of textile mesh was embedded such that rovings were arranged in the length and width directions of the specimen at a height of 10 mm from the bottom of the specimen. As with the pull-out specimen, the edge of the textile mesh was fixed to the mold in advance, and care was taken to avoid applying prestress to the textile mesh during fixing. The TRM specimens were demolded 24 h after casting, followed by curing in water for 28 days at 20 ± 0.5 °C.

Figures 4 and 5 show the geometry of the test specimen and the experimental setup for the four-point bending test. The length of the clear span was 300 mm, and the load was applied under displacement control at a speed of 0.2 mm/min at the two trisection points between the clear span. Because the LVDT was installed in the center of the lower surface of the specimen, the deflection measured during the test corresponded to that at this position. The applied load and deflection were measured and recorded every second using a data logger.
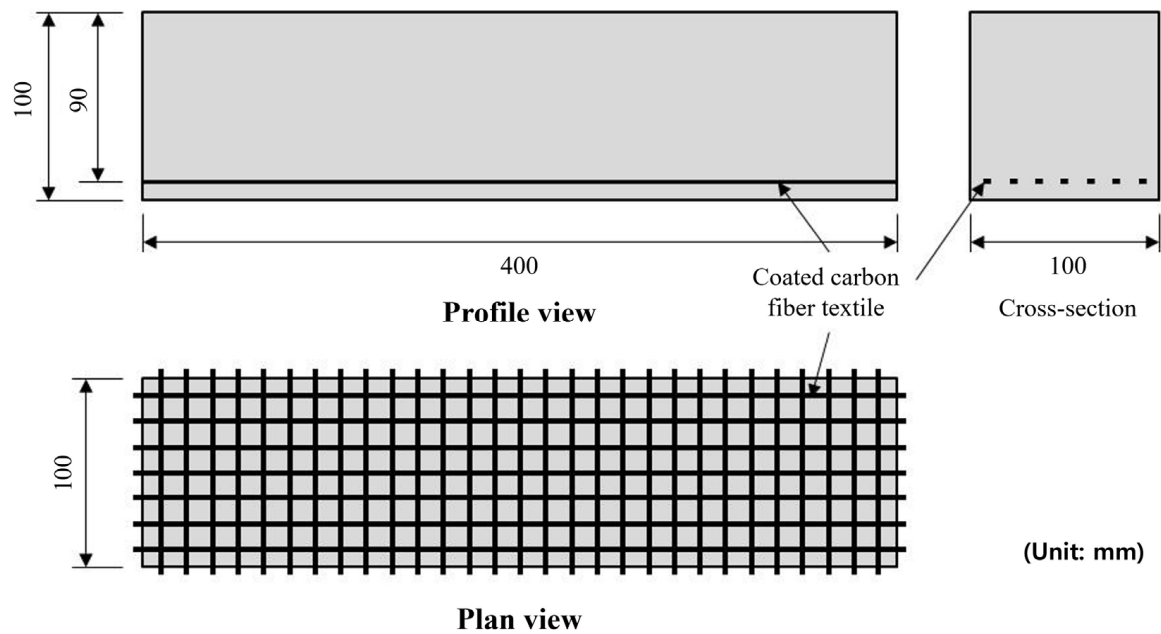
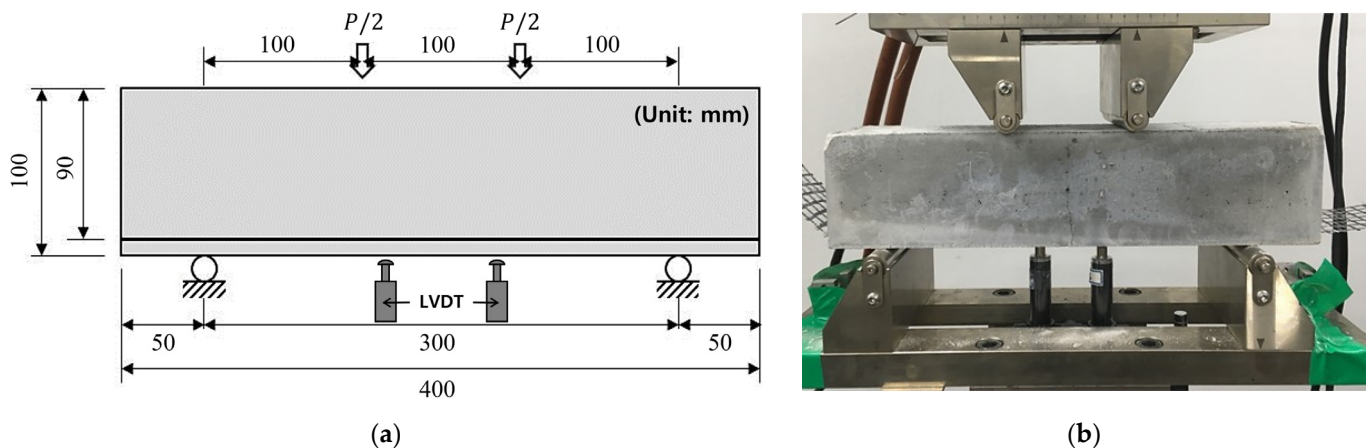**Figure 4.** Specimen geometry for the four-point bending test.

Figure 5. Experimental setup for the four-point bending test. (**a**) Schematics and (**b**) test specimen mounted on a universal testing machine with bending jigs.

3. Experimental Results and Discussion

3.1. Pull-Out of Textile Reinforcement in Cement Composites

Figure 6 shows the relationship between the load and pull-out displacement of the coated carbon-fiber textile reinforcement as measured during the direct pull-out test. The pull-out displacement refers to the mean value of the measured displacement obtained from two LVDTs mounted on both sides of the specimen (see Figure 3). The red line in Figure 6 represents the average measured test results. Noticeably, little pull-out displacement occurred until a pull-out load of approximately 900 N. Thereafter, as the fiber textile was gradually pulled, the load and pull-out displacement gradually increased. This is attributed to the adhesion bond in the textile–cement matrix interfacial zone being dominant during the beginning stage of the test, whereas the adhesion became increasingly limited as the pull-out displacement increased. Accordingly, the pull-out behavior was dominated by the bond strength between the fiber textile and the cement matrix [41]. The average pull-out load peaked at approximately 1256 N at a pull-out displacement of approximately 0.92 mm, which differs from the predictable tensile force of roving from Table 2. This difference is attributed to the gradual slip of fiber roving from the specimen as the load

increased, which resulted in a decrease in tensile performance compared to the ideal direct tensile strength without slipping (Table 2). In addition, there is some uncertainty regarding the roving geometry. After that, the load decreased rapidly to approximately 292 N until the displacement reached approximately 1 mm, and the load decreased slightly as the displacement increased, as shown in Figure 6. This is attributed to a sharp decrease in the pull-out force with increasing slip between the cement matrix and the textile, which is called the pure friction phase [42]. In addition, a part of the fiber textile was ruptured. This confirms that the TRM withstood low loads under the bond action of some fibers that were not ruptured within the slipping region.
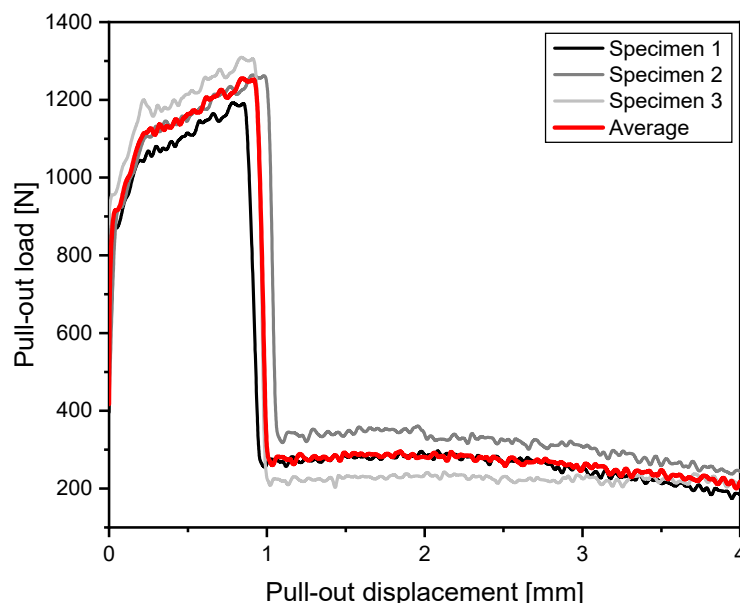

Figure 6. Load–displacement response of the pull-out test.

　　　Although the geometry of the rovings was not exactly the same and the pull-out test was conducted on three specimens, the experimental results are considered to be representative because all specimens exhibit very similar behavior. This indicates that the geometry of the tested rovings was not much different.

　　　The shape of the local bond stress–slip function depends on the compressive strength of the concrete, the perimeter of the textile roving, and the configuration of the mesh cross-threads [21]. In pull-out tests involving ribbed rebars with an embedded length of less than five times the diameter, the stress distribution along the rebar was assumed to be uniform. Although the behavior of textile reinforcement may differ slightly from that of rebar due to the heterogeneity of the roving, according to an existing study [21], the assumptions for rebar can be applied to simplify the analysis of the overall bond behavior, such as the bond stress–slip behavior of textile reinforcement. Therefore, according to the experimental results of the load–slip behavior, the bond stress of the textile reinforcement can be calculated from Equation (1):

$$\tau = \frac{P}{p_r(L_e - s)} \tag{1}$$

where P, L_e, p_r, and s denote the applied load, embedded length, roving perimeter, and pull-out displacement of fiber roving measured using LVDTs, respectively.

　　　Figure 7 shows the bond stress–slip behavior of the coated carbon-fiber textile reinforcement determined from Equation (1). Here, p_r was the value provided by the manufacturer, as listed in Table 2. The average value (red line in Figure 6) was utilized as the measured value because the pull-out behaviors of each test specimen were similar, as shown in Figure 6. As described above, the effect of the adhesive bond was dominant when the slip

was very small. On the other hand, the bond stress increased as the initial slip increased, and the bond stress rapidly decreased when the fiber ruptured after reaching the maximum strength. The maximum bond stress of one roving was approximately 13.44 MPa when 0.92 mm of slip occurred, as shown in Figure 7.
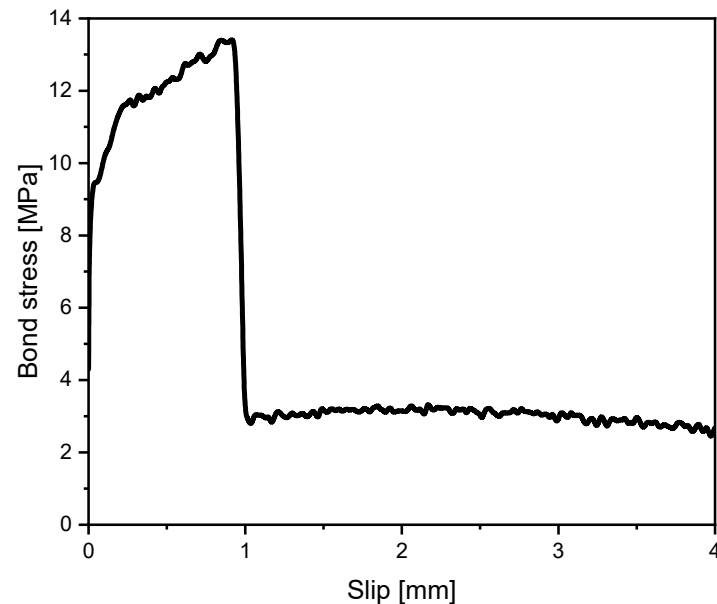

Figure 7. Bond stress–slip response.

The geometry of the textile may affect its reinforcing efficiency in the TRM. For example, textiles with relatively complicated yarn shapes, such as short weft knit, may enhance the bonding and improve the performance of composites [43]. Because the bond stress–slip behavior in this study was limited to textiles with specific geometry, further studies are needed to determine the effect of textile texture on the bond behavior in cementitious materials.

3.2. Flexural Load–Displacement Response of the TRM

Figure 8 shows the load–deflection behavior measured through the four-point bending tests conducted on the TRM specimens. Noticeably, the deflection increased proportionally with the load increase at the beginning of the experiment. When the load reached 12–15 kN, dominant flexural cracks occurred at the bottom center of the beam specimens. Meanwhile, as flexural cracks occurred, the loads decreased to some extent due to the loss of tensile stress in the mortar beams but gradually increased due to the bond behavior of the textile reinforcement across the cracks during the subsequent pull-out process. Thereafter, the crack width increased, and the crack gradually propagated to the top of the specimen as the deflection and load increased. Most specimens were confirmed to be incapable of bearing load after peak load was reached, as shown in Figure 8. This is attributable to the occurrence of brittle fracture after the fibers exposed to the cracks raptured. The maximum loads at the fracture of the specimens were 15.1–22.2 kN. Although the maximum loads varied, the general load–deflection responses before fracture in all specimens were roughly similar. The flexural load in one specimen gradually decreased after the maximum load was reached, in contrast to the behavior of other specimens, where the bending test ended immediately after the maximum load was reached. Presumably, the fiber rovings of textile exposed to the crack raptured gradually rather than suddenly as the load increased; hence, the observation in the former specimen.
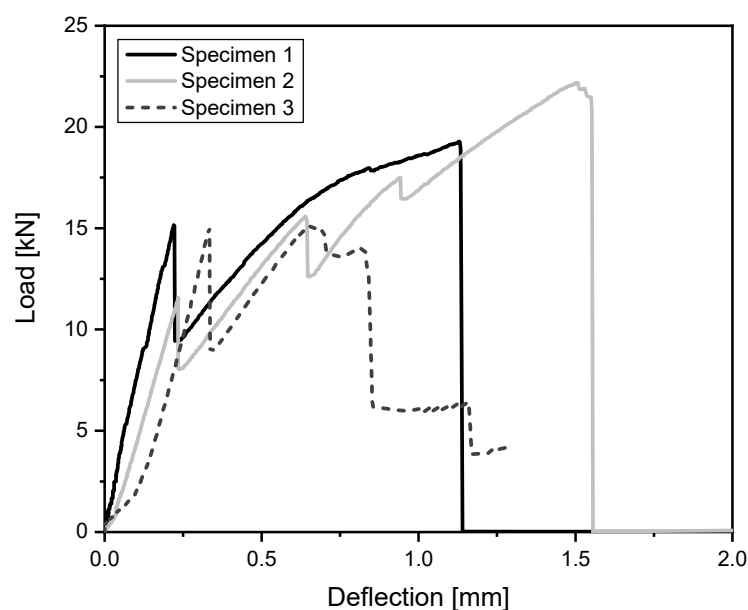
Figure 8. Load–deflection curves from four-point bending test.

Although the bending test was conducted on three TRM specimens, and some variations were present in the peak load between the specimens, the flexural behavior of all specimens tended to be similar. Accordingly, the experimental results are deemed to represent the overall flexural behavior of the TRM used.

The nominal flexural strength (f) was calculated using Equation (2) [29]:

$$f = \frac{PL}{bh^2} \tag{2}$$

where P, L, b, and h denote load, span length, beam width, and beam height, respectively. Flexural toughness (f_e) refers to the capacity to support load past cracking and is expressed as the equivalent flexural strength. Specifically, it denotes the toughness obtained from the load–deflection curve until the deflection of the loading point is $L/150$ of the span [40]; it was calculated from Equation (3) [44]:

$$f_e = \frac{T_b L}{\delta_{tb} bh^2} \tag{3}$$

Table 3 lists the flexural properties of the TRM specimens, including load, deflection, flexural strength, and flexural toughness. Although the test results vary, the ultimate strengths of all TRM specimens were higher than the first-crack strengths, as presented in Figure 8 and Table 3. The mean value of the ultimate strengths was 5.66 ± 1.06 MPa, which was an increase of approximately 36% compared to that of the first-crack strengths of 4.17 ± 0.61 MPa. In addition, the mean flexural toughness was 2.49 ± 0.87 MPa. These results reveal that the coated carbon-fiber textile improved the flexural properties of the cracked mortar beam. In this respect, textile is considered an effective reinforcement for enhancing the tensile performance of concrete after cracking.

Table 3. Flexural behavior of TRM specimens.

Specimen	First-Crack Load [kN]	Ultimate Load [kN]	First-Crack Strength [MPa]	Ultimate Strength [MPa]	Ultimate Deflection [mm]	Flexural Toughness [MPa]
1	15.16	19.28	4.55	5.79	1.128	2.42
2	11.57	22.18	3.47	6.66	1.508	3.40
3	15.02	15.13	4.49	4.54	0.657	1.66

4. Analysis for the Flexural Behavior

4.1. Idealization of the Flexural Behavior

During the four-point bending test, the TRM beams eventually fractured as the dominant crack formed at the bottom center gradually propagated. When a beam fractures due to one dominant flexural crack, the flexural behavior can be briefly analyzed by idealizing the deformation and failure modes of the flexural member, as shown in Figure 9 [45–47].
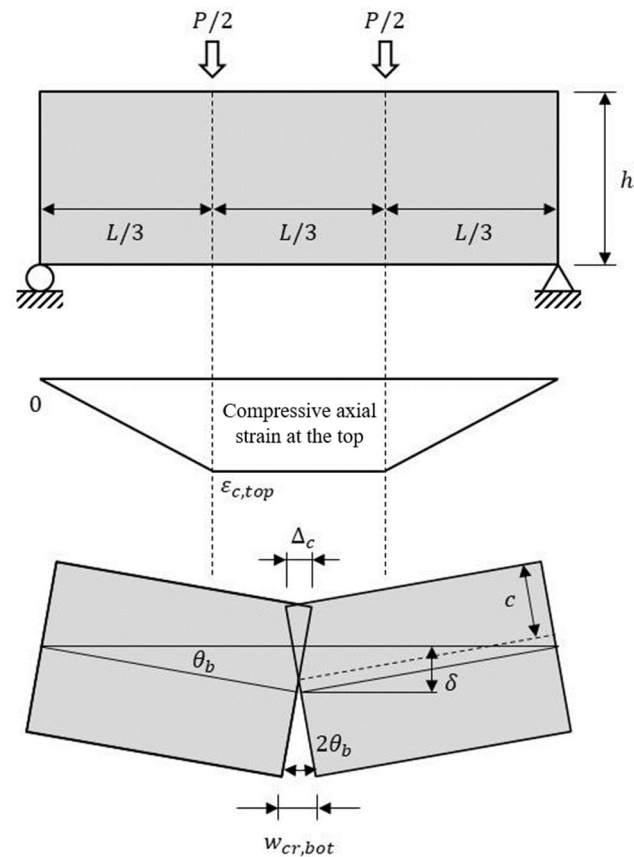

Figure 9. Idealized failure mode of coated carbon-fiber-textile-reinforced beam.

From the failure mode shown in Figure 9, the relationship between compressive axial strain at the top of the section ($\varepsilon_{c,top}$) and compressive deformation at the top surface (Δ_c) can be calculated, as given in Equation (4) [46]. Note that Δ_c is the compressive deformation through the top surface within the pure span.

$$\Delta_c = \int_0^L \varepsilon_{x,top} dx = \frac{2}{3} \varepsilon_{c,top} L \tag{4}$$

From the geometric condition shown in Figure 9, the flexural crack width at the bottom of the beam ($w_{cr,bot}$) is $2\theta_b(h-c)$ and $\theta_b = \Delta_c/2c$. Incorporating this into Equation (4), the relationship between $\varepsilon_{c,top}$ and $w_{cr,bot}$ is derived as follows:

$$\varepsilon_{c,top} = \frac{3c}{2L(h-c)} w_{cr,bot} \tag{5}$$

where c denotes the distance from the top surface to the neutral axis in the beam cross-section.

In addition, assuming that the coated carbon-fiber textile reinforcement is embedded at the effective depth (d_f) in the cross-section of the beam (see Figure 10), the crack width

at the embedded depth of the coated carbon-fiber textile reinforcement ($w_{cr,f}$) can be calculated for $w_{cr,bot}$ as follows:
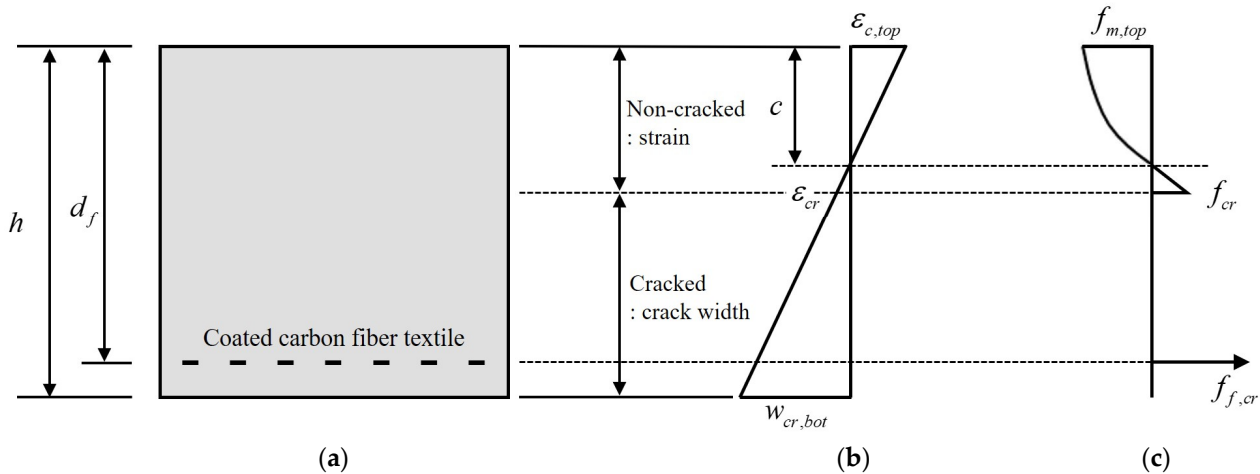
$$w_{cr,f} = \frac{d_f - c}{h - c} w_{cr,bot} \tag{6}$$

Figure 10. Stress–strain distribution across TRM beam depth. (**a**) Beam cross-section, (**b**) strain and crack width diagram, and (**c**) stress diagram.

Therefore, the relationship between $w_{cr,f}$ and the deflection at the center of the beam (δ) can be rewritten from Equations (4)–(6), as follows:

$$\delta = \frac{L}{4(d_f - c)} w_{cr,f} \tag{7}$$

4.2. Stress Distribution and Internal Moment at the Critical Section

Figure 10 shows the stress–strain distribution in the cross-section of the cracked TRM beam. From the relationship in Equation (5), the strain and crack width distributions along the cross-section depth at the cracks can be expressed, as shown in Figure 10b. In the noncracked section, the compressive stress of the cement mortar is distributed for a given strain. On the other hand, the tensile stress in the cracked section caused by the cement mortar is zero, and only the tensile stress caused by the coated carbon-fiber textile reinforcement exists, as shown in Figure 10c.

Therefore, the sectional moment M can be calculated from the stress distribution in the cross-section of the TRM beam. Moreover, the load applied to the TRM beam can be calculated from Equation (8):

$$P = \frac{6M}{L} \tag{8}$$

4.3. Constitutive Relations

Figure 11 shows the compressive stress–strain relationship in the noncracked section, which is determined from the relation proposed in a previous study [48]. The parabolic part of the curve can be calculated from Equation (9), which is valid until the stress reaches $0.9 f'_m$ in the descending part.

$$f_m = f'_m \left[\frac{2\varepsilon_m}{\varepsilon'_m} - \left(\frac{\varepsilon_m}{\varepsilon'_m} \right)^2 \right] \quad for \quad 0 < \varepsilon'_m < \varepsilon_m \ (at\ 0.9\ f'_m) \tag{9}$$

where f_m denotes the compressive stress, f'_m denotes the peak stress, ε_m denotes the compressive strain, and ε'_m denotes the peak strain at f'_m.
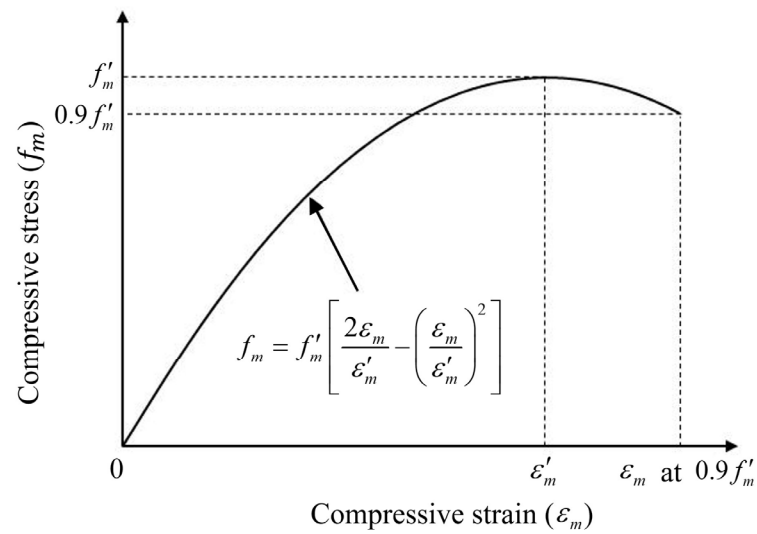
Figure 11. Stress–strain curve of mortar in compression.

The bond stress of the textile mesh inside the TRM beam can be calculated for a given crack width by considering the bond–slip relationship within the cement matrix as calculated from the pull-out test. This relationship was idealized as follows based on a previous study [49]:

$$\tau_s = \tau_{max} \left(\frac{s_x}{s_1} \right)^{\alpha} \tag{10}$$

where τ_s denotes the bond stress when slip s_x occurs, τ_{max} denotes the maximum bond strength, s_1 denotes the slip corresponding to τ_{max}, and α denotes an index for the characteristics of bond behavior.

Figure 12 compares the measured value from the pull-out test and the predicted value from Equation (10) for the bond behavior. Noticeably, when τ_{max} was 13.44 MPa, s_1 was 0.92 mm, α was 0.1, and the predicted value almost coincided with the actual bond behavior of the coated carbon-fiber textile reinforcement.
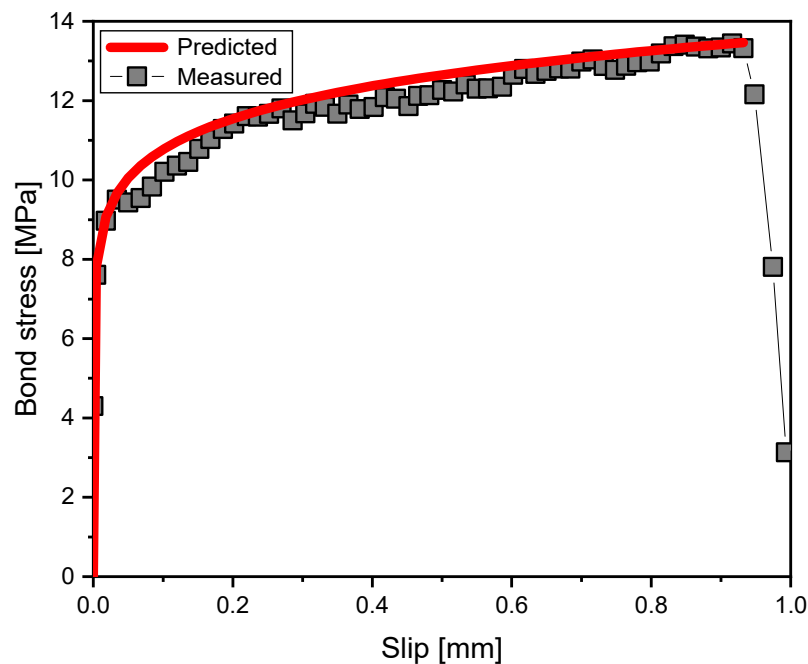

Figure 12. Bond stress–slip relationship: predicted vs. measured for coated carbon-fiber textile reinforcement.

In addition, to calculate the tensile stress in the coated carbon-fiber textile reinforcement ($f_{f,cr}$) for a given crack width ($w_{cr,f}$), the crack width–tensile stress relation from a previous study [50] for reinforced concrete beams was modified as follows:

$$f_{f,cr} = \left[\frac{2kE_f^2 \tau_{max}}{s_1^\alpha (1+\alpha)} \left(\frac{w_{cr,f}}{2} \right)^{1+\alpha} \right]^{1/2} \tag{11}$$

where E_f denotes the modulus of elasticity of the coated carbon-fiber textile reinforcement, (240 GPa). k denotes the coefficient for the stiffness and bond interface for the tensile section and is calculated as follows:

$$k = p_r \left(\frac{1}{E_c A_{c,eff}} + \frac{1}{E_f A_f} \right) \tag{12}$$

where E_c denotes the modulus of elasticity of cement mortar and A_f denotes the cross-sectional area of the coated carbon-fiber textile reinforcement. $A_{c,eff}$ denotes the effective tension area of cement mortar, which can be calculated from Equation (13) [2]:

$$A_{c,eff} = 2.5(h - d_f) \tag{13}$$

Equation (11) is derived as follows. Oh and Kim [50] presented the following equation for a concrete member with a single rebar:

$$\frac{w_{cr}}{2} = \left[\frac{s_1^\alpha d_b (1+\alpha) f_{s,cr}^2}{8(1 + n_E \rho_s) \tau_{max} E_s} \right]^{\frac{1}{1+\alpha}} \tag{14}$$

where d_b denotes the reinforcing bar diameter, $f_{s,cr}$ denotes the reinforcing bar stress at crack, n_E denotes the modular ratio ($= E_s/E_c$), ρ_s denotes the effective reinforcement ratio ($= A_s/A_{c,eff}$), and E_s denotes the modulus of elasticity of steel. Equation (14) can be rewritten with $\rho_s = \pi d_b^2 / 4A_c$ and $p_r = \pi d_b$, as follows:

$$\frac{w_{cr}}{2} = \left[\frac{s_1^\alpha (1+\alpha) f_{s,cr}^2}{2p_r \left(\frac{1}{E_c A_{c,eff}} + \frac{1}{E_s A_s} \right) \tau_{max} E_s^2} \right]^{\frac{1}{1+\alpha}} \tag{15}$$

For coated carbon-fiber textile, we can replace $w_{cr} = w_{cr,f}$, $f_{s,cr} = f_{f,cr}$, $E_s = E_f$, and $A_s = A_f$. Hence, $f_{f,cr}$ is calculated for a given $w_{cr,f}$ as follows:

$$f_{f,cr} = \left[2p_r \left(\frac{1}{E_c A_{c,eff}} + \frac{1}{E_f A_f} \right) \frac{E_f^2 \tau_{max}}{s_1^\alpha (1+\alpha)} \left(\frac{w_{cr,f}}{2} \right)^{1+\alpha} \right]^{1/2} \tag{16}$$

The bond behavior of textile reinforcement is directly considered in the flexural analysis in the current analytical work. Equation (10) is the model for representing the bond behavior of the coated carbon-fiber textile. The tensile stress of the coated carbon-fiber textile can be calculated for a given crack width based on Equation (10), as shown in Equation (11). The flexural behavior can then be evaluated. This differs considerably from a conventional section analysis based on the average stress–strain response, which is not appropriate for predicting the flexural behavior of reinforced concrete with a single crack.

Notably, Equation (11) is mathematically derived from Equation (10). Without the bond parameters (τ_{max}, s_1, α) obtained through the pull-out test, predicting the flexural behavior is not feasible, because the stress–crack width relationship from Equation (11) is required.

4.4. Analysis Algorithm

Figure 13 shows the analysis algorithm based on the above description for a mortar beam reinforced with coated carbon-fiber textile. First, the flexural crack width at the bottom of the beam ($w_{cr,bot}$) was set, and the neutral axis position of the cross-section with the set crack width (c) was assumed. Accordingly, the strain distribution of the section was calculated. From the calculated strain distribution, the compressive stress of the cement mortar and the tensile stress of the coated carbon-fiber textile reinforcement ($f_{f,cr}$) in the cracked section can be calculated, and the validity of the assumed neutral axis position can be verified through the equilibrium condition of the forces within the cross-section, as shown in Figure 13. The neutral axis position that satisfies the equilibrium condition within the cross-section can then be determined iteratively, and the sectional moment (M) and the applied load (P) to the beam can then be calculated. Finally, by calculating the deflection at the center of the beam for a given crack width ($w_{cr,f}$), the load–deflection curve of the TRM beam can be predicted.
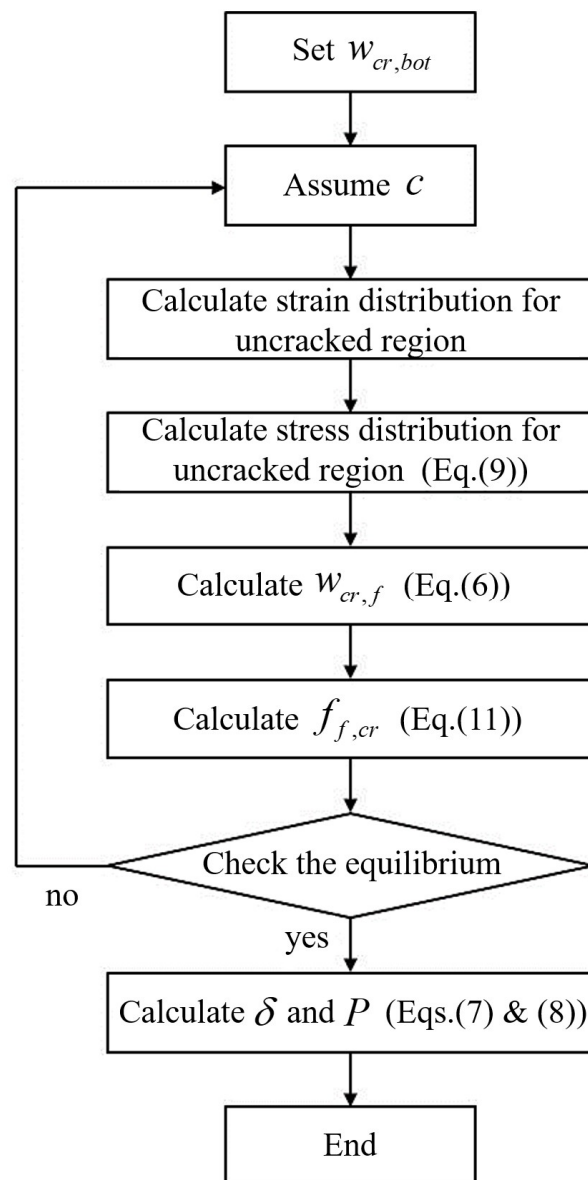

Figure 13. Flow chart for theoretical analysis.

4.5. Comparison with the Test Results

Figure 14 shows the values predicted through the theoretical analysis (as in Figure 13) and the measured values for the load–deflection relationship of the mortar beam reinforced with coated carbon-fiber textile. The entirety of the red curve in Figure 14 was predicted by the model, and the three red points only represent the status corresponding to particular tensile stresses of the coated carbon-fiber textile. As shown in Figure 14, the predicted value of the flexural behavior of the TRM beam after cracking due to the reinforcing effect of the coated carbon-fiber textile was generally consistent with the measured value. However, the flexural rigidity of the TRM beam before the occurrence of flexural cracks predicted in the analysis was higher than that in the experimental results. This difference is attributed to the idealization of the behavior of flexural members in the analysis technique utilized in this study. Although some inconsistencies were present between the predicted and measured flexural behavior of the TRM beam before cracking, the proposed theoretical analysis can effectively predict the flexural behavior of the cracked TRM beam and the reinforcement effect of the coated carbon-fiber textile within reasonable limits. In addition, the pull-out test results are considered reliable because the theoretical analysis was based on the measured bond behavior of the coated carbon-fiber textile reinforcement.
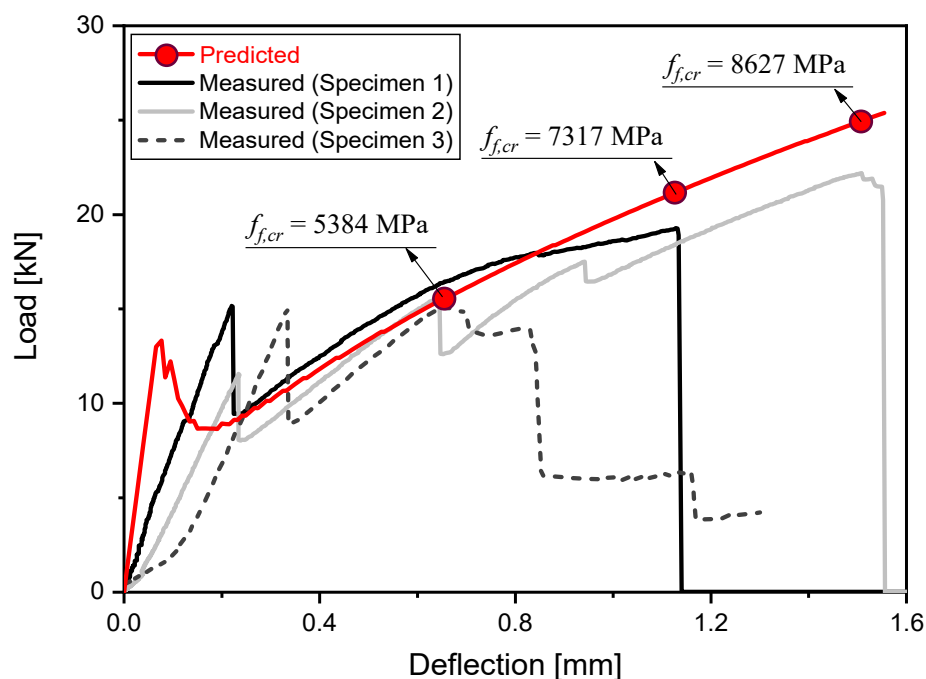

Figure 14. Load–deflection relationship: predicted vs. measured for the mortar beam reinforced with coated carbon-fiber textile.

As shown in Figures 8 and 14, despite the specimens being replicated, variations between the experimentally measured load and deflection values for the TRM failure beam were present. This is attributed to all the textile rovings exposed to the crack not rupturing simultaneously; rather, they ruptured sequentially from the weakest roving, which affected the flexural properties (strength, toughness, etc.) of the TRM beam. In addition, differences in the material properties, such as the tensile strength of each textile or variation in the bond of each roving with the matrix among the load-aligned textile rovings, may have been present. Therefore, for a more detailed analysis, the tensile strength of the textile reinforcement exposed to the crack was predicted through theoretical analysis by utilizing the deflection value at the maximum load for each specimen measured in the actual bending test. The predicted values are shown as red circles in Figure 14. The evaluated tensile strengths were confirmed to have exceeded 4300 MPa, which corresponded to the strength of the textile roving provided by the manufacturer (Table 2). This indicates that using

textiles is advantageous in terms of tensile strength as compared to using individual fibers. However, the tensile strength of the fiber may be uncertain, because the material properties of fibers are generally provided conservatively by manufacturers. The tensile strength of the used textile reinforcement in the cracked section is considered to be at least more than 5384 MPa, as shown in Figure 14.

As shown in Figure 14, predicting the exact point of fracture of the textile using the proposed theoretical analysis is difficult, because variations were present in the measured flexural behavior of TRM beams and the tensile strength of the textile reinforcements. Nevertheless, the flexural behavior and maximum tensile strength of the TRM beam can be predicted conservatively through theoretical analysis by applying the provided tensile properties of the textile fiber. However, for a more reasonable prediction, further comparison between the measured and predicted results is required under various test conditions, considering the limitation in the experimental results on the flexural behavior of the TRM beam in this study. Therefore, further studies in this direction are needed.

5. Conclusions and Discussion

In this study, experimental and theoretical analyses were conducted on the structural behavior of a cement composite reinforced with a coated carbon-fiber textile. A pull-out test was performed to analyze the bond behavior of the coated carbon-fiber textile, and the flexural behavior was analyzed through a four-point bending test on the TRM beam. Moreover, the experimental results were compared with those predicted through theoretical analysis. The major conclusions drawn from this study are as follows:

- The bond stress–slip behavior of coated carbon-fiber textile embedded in the cementitious materials was investigated through a double-sided unsymmetrical pull-out test. Test results demonstrated that the adhesion bond in the textile–cement matrix interfacial zone was initially dominant, but the pull-out behavior came to increasingly rely on the bond strength between the textile and the cement matrix as the pull-out displacement increased. The mean maximum bond stress was approximately 13.44 MPa when slip reached approximately 0.92 mm.
- In the four-point bending test for the TRM beam, as the load increased, the dominant flexural crack gradually developed in the bottom-center of the beam specimen. Finally, brittle fracture occurred due to the rupture of the coated carbon-fiber textile exposed to the crack. The load temporarily decreased immediately after cracking, but the load gradually increased until fracture, because the ductility of the TRM beam was secured by the bond behavior of the textile in the tensile zone. The mean ultimate strength of the TRM beam increased by approximately 36% compared to the mean first-crack strength. This confirmed that the textile used was effective as a reinforcement for improving the tensile performance of cementitious materials after cracking.
- A theoretical analysis method capable of predicting the flexural behavior of the TRM beam was established by idealizing the failure mode based on the actual bond behavior of textile reinforcement in cementitious materials. A comparison of measured and predicted results confirmed that the proposed analysis method can effectively predict the flexural behavior of the cracked TRM beam.

Predicting the structural behavior of the TRM is crucial for its practical application. The theoretical analysis method proposed in this study is expected to be useful because it can be easily implemented in currently available analysis models or tools. However, errors may be present in evaluating the behavior of the TRM beam before cracking, and predicting the exact point of textile facture may not be feasible. Therefore, further studies are required to improve the analysis method through a comparison between the measured and predicted results under various experimental conditions.

Furthermore, the results of current and previous studies suggest that the use of continuous fiber textile as a strengthening material and future structural applications of the TRM beam are feasible. However, regarding field applications of the TRM beam, a more extensive analysis (change in performance according to the texture mesh and mixture

compositions, influence of similar fibers, etc.) is required, along with a comparison of the performance achieved when using rebar and textiles as reinforcement.

Moreover, although this study obtained representative experimental results despite the small number of test specimens, the authors plan to further validate the experimental results and theoretical analysis model through follow-up studies on more samples.

Data Availability Statement: Data will be made available on request.

References

1. ACI Committee. *Building Code Requirements for Structural Concrete (ACI 318-08) and Commentary*; American Concrete Institute: Farmington Hills, MI, USA, 2008.
2. *BS EN 1992-1-1:2004*; Eurocode 2: Design of Concrete Structures. General Rules and Rules for Buildings. British Standards Institute: London, UK, 2004.
3. Duprat, F. Reliability of RC Beams Under Chloride-Ingress. *Constr. Build. Mater.* **2007**, *21*, 1605–1616. [CrossRef]
4. Mehta, P.; Monteiro, P. *Concrete: Microstructure, Properties and Materials*, 3rd ed.; McGraw Hill: New York, NY, USA, 2006.
5. Neville, A.M. *Properties of Concrete*; Wiley: New York, NY, USA, 1996.
6. Yoon, S.; Wang, K.; Weiss, W.J.; Shah, S.P. Interaction between loading, corrosion, and serviceability of reinforced concrete. *ACI Mater. J.* **2000**, *97*, 637–644.
7. Triantafyllou, G.G.; Rousakis, T.C.; Karabinis, A.I. Analytical assessment of the bearing capacity of RC beams with corroded steel bars beyond concrete cover cracking. *Compos. Part B Eng.* **2017**, *119*, 132–140. [CrossRef]
8. Zollo, R.F. Fiber-reinforced concrete: An overview after 30 years of development. *Cem. Conc. Compos.* **1997**, *19*, 107–122. [CrossRef]
9. Yoo, D.-Y.; Banthia, N. Impact resistance of fiber-reinforced concrete—A review. *Cem. Conc. Compos.* **2019**, *104*, 103389. [CrossRef]
10. Hegger, J.; Voss, S. Investigations on the Bearing Behaviour and Application Potential of Textile Reinforced Concrete. *Eng. Struct.* **2008**, *30*, 2050–2056. [CrossRef]
11. Koutas, L.N.; Tetta, Z.; Bournas, D.A.; Triantafillou, T.C. Strengthening of Concrete Structures with Textile Reinforced Mortars: State-of-the-Art Review. *J. Compos. Constr.* **2019**, *23*, 03118001. [CrossRef]
12. Mercuri, M.; Vailati, M.; Gregori, A. Lime-based mortar reinforced with randomly oriented polyvinyl-alcohol (PVA) fibers for strengthening historical masonry structures. *Dev. Built. Environ.* **2023**, *14*, 100152. [CrossRef]
13. Vailati, M.; Mercuri, M.; Angiolilli, M.; Gregori, A. Natural-fibrous lime-based mortar for the rapid retrofitting of heritage masonry buildings. *Fibers* **2021**, *9*, 68. [CrossRef]
14. Angiolilli, M.; Gregori, A.; Vailati, M. Lime-based mortar reinforced by randomly oriented short fibers for the retrofitting of the historical masonry structure. *Materials* **2020**, *13*, 3462. [CrossRef]
15. Thong, C.C.; Teo, D.C.L.; Ng, C.K. Application of polyvinyl alcohol (PVA) in cement-based composite materials: A review of its engineering properties and microstructure behavior. *Constr. Build. Mater.* **2016**, *107*, 172–180. [CrossRef]
16. Ticoalu, A.; Aravinthan, T.; Cardona, F. A review of current development in natural fiber composites for structural and infrastructure applications. In Proceedings of the Southern Region Engineering Conference (SREC 2010), Toowoomba, Australia, 10–12 November 2010; pp. 113–117.
17. Shams, A.; Horstmann, M.; Hegger, J. Experimental investigations on Textile-Reinforced Concrete (TRC) sandwich sections. *Compos. Struct.* **2014**, *118*, 643–653. [CrossRef]
18. Portal, N.W.; Flansbjer, M.; Johannesson, P.; Malaga, K.; Lundgren, K. Tensile behaviour of textile reinforcement under accelerated ageing conditions. *J. Build. Eng.* **2015**, *5*, 57–66. [CrossRef]
19. Lee, S.-C.; Oh, J.-H.; Cho, J.-Y. Fiber orientation factor on rectangular cross-section in concrete members. *Int. J. Eng. Technol.* **2015**, *7*, 470–473.
20. Lee, S.-C.; Oh, J.-H.; Cho, J.-Y. Fiber efficiency in SFRC members subjected to uniaxial tension. *Constr. Build. Mater.* **2016**, *113*, 479–487. [CrossRef]

21. Portal, N.W.; Perez, I.F.; Thrane, L.N.; Lundgren, K. Pull-out of textile reinforcement in concrete. *Constr. Build. Mater.* **2014**, *71*, 63–71. [CrossRef]
22. Naser, M.Z.; Hawileh, R.A.; Abdalla, J.A. Fiber-reinforced polymer composites in strengthening reinforced concrete structures: A critical review. *Eng. Struct.* **2019**, *198*, 109542. [CrossRef]
23. Bielak, J.; Li, Y.; Hegger, J.; Chudoba, R. Characterization procedure for bond, anchorage and strain-hardening behavior of textile-reinforced cementitious composites. In Proceedings of the 18th International Conference on Experimental Mechanics (ICEM 2018), Brussels, Belgium, 1–5 July 2018; p. 395.
24. Goliath, K.B.; Cardoso, D.C.; Silva, F.D.A. Flexural behavior of carbon-textile-reinforced concrete I-section beams. *Compos. Struct.* **2021**, *260*, 113540. [CrossRef]
25. Portal, N.W.; Lundgren, K.; Walter, A.M.; Frederiksen, J.O.; Thrane, L.N. Numerical modelling of textile reinforced concrete. In Proceedings of the 8th International Conference on Fracture Mechanics of Concrete and Concrete Structures (FraMCoS 2013), Toledo, Spain, 11–14 March 2013; pp. 886–897.
26. Portal, N.W.; Thrane, L.N.; Lundgren, K. Flexural behaviour of textile reinforced concrete composites: Experimental and numerical evaluation. *Mater. Struct. Constr.* **2017**, *50*, 4. [CrossRef]
27. Portal, N.W.; Flansbjer, M.; Zandi, K.; Wlasak, L.; Malaga, K. Bending behaviour of novel textile reinforced concrete-foamed concrete (TRC-FC) sandwich elements. *Compos. Struct.* **2017**, *177*, 104–118. [CrossRef]
28. Yin, S.P.; Xu, S.L.; Wang, F. Investigation on the flexural behavior of concrete members reinforced with epoxy resin-impregnated textiles. *Mater. Struct.* **2015**, *48*, 153–166. [CrossRef]
29. Du, Y.; Zhang, X.; Zhou, F.; Zhu, D.; Zhang, M.; Pan, W. Flexural behavior of basalt textile-reinforced concrete. *Constr. Build. Mater.* **2018**, *183*, 7–21. [CrossRef]
30. *ISO 679*; Cement-Test Methods-Determination of Strength. International Organization for Standardization (ISO): Geneva, Switzerland, 2009.
31. *ASTM C873/C873M*; Standard Test Method for Compressive Strength of Concrete Cylinders Cast in Place in Cylindrical Molds. American Society for Testing and Materials (ASTM): West Conshohocken, PA, USA, 2015.
32. *ASTM C469/C469M*; Standard Test Method for Static Modulus of Elasticity and Poisson's Ratio of Concrete in Compression. American Society for Testing and Materials (ASTM): West Conshohocken, PA, USA, 2014.
33. Triantafillou, T. *Textile Fibre Composites in Civil Engineering*, 1st ed.; Woodhead Publishing: Sawston, UK, 2016.
34. Barhum, R.; Mechtcherine, V. Effect of short, dispersed glass and carbon fibres on the behaviour of textile-reinforced concrete under tensile loading. *Eng. Fract. Mech.* **2012**, *92*, 56–71. [CrossRef]
35. Barhum, R.; Mechtcherine, V. Influence of short dispersed and short integral glass fibres on the mechanical behaviour of textile-reinforced concrete. *Mater. Struct.* **2013**, *46*, 557–572. [CrossRef]
36. Zastrau, B.; Richter, M.; Lepenies, I. On the Analytical Solution of Pullout Phenomena in Textile Reinforced Concrete. *J. Eng. Mater. Technol.* **2003**, *125*, 38–43. [CrossRef]
37. Banholzer, B. Bond of a strand in a cementitious matrix. *Mater. Struct.* **2006**, *39*, 1015–1028. [CrossRef]
38. Lorenz, E.; Ortlepp, R. Bond behavior of textile reinforcements-development of a pull-out test and modeling of the respective bond versus slip relation. In *High Performance Fiber Reinforced Cement Composites 6*; Parra-Montesinos, G.J., Reinhardt, H.W., Naaman, A.E., Eds.; Springer: Dordrecht, The Netherlands, 2012; Volume 2, pp. 479–486.
39. Krüger, M. Vorgespannter Textilbewehrter Beton. Ph.D. Thesis, University of Stuttgart, Stuttgart, Germany, 2004.
40. *ASTM C1609/C1609M*; Standard Test Method for Flexural Performance of Fiber-Reinforced Concrete(Using Beam with Thrid-Point Loading. American Society for Testing and Materials (ASTM): West Conshohocken, PA, USA, 2012.
41. Richter, M.; Lepenies, I.; Zastrau, B.W. On the influence of the bond behaviour between fiber and matrix on the material properties of textile reinforced concrete. In Proceedings of the International Symposium of Anisotropic Behaviour of Damaged Materials, Krakow, Poland, 9–11 September 2002; Volume 1, pp. 1–24.
42. Tran, M.T.; Vu, X.H.; Ferrier, E. Experimental and numerical investigation of carbon textile/cementitious matrix interfacebehaviourfrom pull-out tests. *Constr. Build. Mater.* **2021**, *282*, 122634. [CrossRef]
43. Peled, A.; Bentur, A. Fabric structure and its reinforcing efficiency in textile reinforced cement composites. *Compos. Part A* **2003**, *34*, 107–118. [CrossRef]
44. Kim, D.J.; Naaman, A.E.; El-Tawil, S. Comparative flexural behavior of four fiber reinforced cementitious composites. *Cem. Concr. Compos.* **2008**, *30*, 917–928. [CrossRef]
45. Oh, B.H.; Park, D.G.; Kim, J.C.; Choi, Y.C. Experimental and theoretical investigation on the postcracking inelstic behavior of synthetic fiber reinforced concrete beams. *Cement Concr. Res.* **2005**, *35*, 384–392.
46. Lee, S.-C.; Cho, J.-Y.; Vecchio, F.J. Simplified diverse embedment model for steel fiber-reinforced concrete elements in tension. *ACI Mater. J.* **2013**, *110*, 403–412.
47. Lee, S.-C. Re-evaluation of fibre-reinforced concrete tension model in CEB-FIP Model Code 2010. *Mater. Res. Inno.* **2015**, *19*, S8-107–S8-110. [CrossRef]
48. Kaushik, H.B.; Rai, D.C.; Jain, S.K. Stress-strain characteristics of clay brick masonry under uniaxial compression. *J. Mater. Civ. Eng.* **2007**, *19*, 728–739. [CrossRef]

49. Balázs, G.L. Cracking analysis based on slip and bond stresses. *ACI Mater. J.* **1993**, *90*, 340–348.
50. Oh, B.H.; Kim, S.H. Advanced crack width analysis of reinforced concrete beams under repeated loads. *J. Struct. Eng.* **2007**, *133*, 411–420. [CrossRef]